

1 Modelling Convection Over Arctic Leads With LES 2 and a Non-Eddy-Resolving Microscale Model

C. Lüpkes,¹ V.M. Gryanik,^{1,2} B. Witha,³ M. Gryschka,³ S. Raasch,³ and T.

Gollnik¹

3 published in:

4 J. Geophys. Res., 113, C09028, doi:10.1029/2007JC004099

C. Lüpkes, Alfred Wegener Institute for Polar and Marine Research, Postfach 120161, D-27515 Bremerhaven, Germany. (Christof.Luepkes@awi.de)

¹Alfred Wegener Institute for Polar and Marine Research, Bremerhaven, Germany

²A.M. Obukhov Institute of Atmospheric Physics, Russian Academy of Sciences, Moscow, Russia

³Institute of Meteorology and Climatology, University of Hannover, Germany

5 **Abstract.** Turbulent heat transport over inhomogeneous surfaces with
6 sharp temperature discontinuities is investigated with a focus on the flow over
7 leads in sea ice. The main goal consists in the development of a turbulence
8 closure for a microscale atmospheric model resolving the integrated effect of
9 plumes emanated from leads, but not the individual convective eddies. To
10 this end ten runs are carried out with a Large Eddy Simulation (LES) model
11 simulating the flow over leads for spring time atmospheric conditions with
12 near-neutral inflow and a strong capping inversion. It is found that leads con-
13 tribute to the stabilizing of the polar atmospheric boundary layer (ABL) and
14 that strong countergradient fluxes of heat exist outside a core region of the
15 plumes. These findings form the basis for the development of the new clo-
16 sure. It uses a new scaling with the internal ABL height and the character-
17 istic vertical velocity for the plume region as the main governing parame-
18 ters. Results of a microscale model obtained with the new closure agree well
19 with the LES for variable meteorological forcing in case of lead-orthogonal
20 flow and for a fixed ABL height and lead width. The good agreement con-
21 cerns especially the plume inclination, temperature and heat fluxes as well
22 as the relative contributions of gradient and countergradient transport of heat.
23 A future more general closure should account e.g., for variable lead widths
24 and wind directions. Results of the microscale model could be used to de-
25 rive a future parameterization of the lead effect in large scale models.

1. Introduction

26 A large part of the Arctic Ocean is covered permanently with pack ice. But due to
27 divergent sea ice drift, even during winter open water areas exist, which are called leads or
28 polynyas depending on their shape. The length of leads varies between hundreds of meters
29 and hundreds of kilometers, and their width ranges from several meters to kilometers. A
30 typical sea ice situation in springtime is displayed in Figure 1 by an image of the satellite
31 Aqua Modis obtained on 16 April 2005 about 100 km northeast of Svalbard. The three
32 largest leads in this image have a length of approximately 150 km. Leads are either free of
33 ice or at least covered by thin new ice only. Between late autumn and spring the surface
34 temperature of open water and of new thin ice is much larger than the air temperature.
35 Due to the large temperature differences of up to 40 K, strong turbulent convection is
36 generated above the leads, which penetrates into the slightly stable or neutral shallow
37 atmospheric polar boundary layer, and thus, significantly modifies its structure.

38 Since leads are observed everywhere in the pack ice and at any season, they can have
39 a large influence on the energy exchange between the polar ocean and the atmosphere
40 [Lüpkes *et al.*, 2008]. With respect to climate modelling it seems necessary to gain a
41 detailed understanding of the atmospheric processes in the environment of an ensemble of
42 leads and especially to investigate the transport of heat by convective plumes above and
43 downstream of typical individual leads.

44 Convection above leads has been studied in the past by observations and modelling.
45 Observations and their analysis concentrated mainly on the near-surface processes over
46 leads [Paulson and Smith, 1974; Andreas *et al.*, 1979; Ruffieux *et al.*, 1995; Alam and

47 *Curry, 1997; Persson et al., 1997; Pinto et al., 2003*]. These studies show that there is
48 a strong influence of leads on the downstream near-surface profiles of wind speed and
49 temperature and that heat fluxes over leads range in the order of hundreds of W m^{-2} .
50 Based on data analyses *Andreas and Murphy [1986]* and later *Andreas and Cash [1999]*
51 proposed a parameterization of the surface layer transfer coefficients of heat as a function
52 of the non-dimensional fetch in the lead. They found that coefficients increase with
53 decreasing fetch. The fetch dependence of the surface heat fluxes was confirmed by *Alam*
54 *and Curry [1997]*, who derived the heat transfer coefficients applying surface renewal
55 theory to the air-sea interface. Drag coefficients were derived as a function of various
56 parameters e.g., the wave age, which is also fetch dependent.

57 An improved understanding of the impact of leads on the atmospheric boundary layer
58 (ABL) requires a consideration of processes in the entire ABL rather than of the near-
59 surface processes only. This has been done in the past with high resolution 2D models
60 [*Zulauf and Krueger, 2003*] and with large eddy simulation (LES) models, since observa-
61 tions of the flow across leads were not available with sufficient resolution for a detailed data
62 based analysis of processes. *Glendening and Burk [1992]* as well as *Weinbrecht and Raasch*
63 *[2001]* simulated convective processes with LES above small scale (200 m width) leads for
64 non-zero geostrophic wind, prescribing a stably stratified ABL in the lead environment
65 with a height constant vertical temperature gradient. *Esau [2007]* studied processes over
66 leads of different widths, but for zero geostrophic wind. Conditions in a real arctic en-
67 vironment are often characterized, however, by a slightly stable or close to neutral ABL
68 of 50 m to 500 m thickness, which is capped by a strong inversion. Moreover, in arctic
69 regions strong wind speeds occur much more often than light winds [*Lüpkes et al., 2008*].

70 Thus, the first goal of our present investigation is to model convection with LES over
71 leads using observed inflow profiles with a neutral lower layer capped by an inversion at
72 300 m. We consider conditions with wind speeds strong enough to avoid a recirculation as
73 that modeled by *Esau* [2007]. The lead width will be prescribed to 1 km, which is typical
74 for conditions in the Fram Strait pack ice region [*Lüpkes et al.*, 2004].

75 The second goal is the development of a turbulence closure for microscale modelling of
76 the flow over leads resolving only the integrated effect of plumes emanated from leads but
77 not the individual convective eddies as in LES. This is done for two reasons. The first is
78 that the microscale modelling helps to gain additional insight into the governing processes
79 related to the flow over leads. This is of fundamental importance for the future derivation
80 of parameterizations of the lead influence to be used in climate models. The second reason
81 is that the application of LES models is restricted to a relatively small domain, whereas
82 a microscale model could be used later to investigate the impact of an ensemble of leads
83 in domains much larger than that possible for LES models.

84 We use a 2D-microscale model with 200 m horizontal grid spacing to model the convec-
85 tion over leads with 1 km width similar as *Mauritsen et al.* [2005] in their study of internal
86 gravity wave generation by leads. Convective eddies cannot be resolved with such grid
87 sizes, and a priori, it is not clear, to what extent the results of such a model can be realis-
88 tic. Classical turbulence closures have been developed for horizontally quasi-homogeneous
89 turbulence. However, strong horizontal gradients of wind, temperature, stratification, and
90 turbulent fluxes exist over sea ice with leads. A schematic representation of the typical
91 flow regimes above a lead is given in Figure 2 showing the slightly stable or neutral region
92 upstream of a lead, a tilted plume region with strong convection and an outflow region,

93 which is again slightly stable or neutral. It can be expected that turbulence closures have
94 to be adjusted to the typical atmospheric conditions in such an environment.

95 We will present at the end a closure accounting for this complex flow structure. It is
96 nonlocal in the plume region and local for its close environment. Still, its applicability will
97 be tested for a few idealized cases only, but it can be considered as a first step towards a
98 more general closure to be used in microscale models for convection over inhomogeneous
99 surfaces with sharp temperature discontinuities. This work does not consider, how the
100 effect of leads could be treated in large scale numerical models. However, results of the
101 microscale model could be used in the future to develop parameterizations for such models.
102 This is outlined in Section 7.

103 Overall, our work contains the following topics: a case study with LES of the ABL
104 response on convective heating by leads (i), the development of a new scaling for convective
105 turbulence in the environment of leads and a new parameterization of heat transport above
106 and downstream of leads (ii) and its application to a microscale model (iii). The paper
107 is structured as follows. After a short presentation of the used models (Sections 2 and
108 3), we explain results of the LES model (Section 4), which is applied to model the flow
109 across a lead. Hereafter, in Section 5 the new turbulence closure is derived and results of
110 the microscale model with the new closure are explained in Section 6.

2. Model Description

2.1. The Microscale Model

111 We use the nonhydrostatic and anelastic atmospheric model METRAS [*Schlünzen*, 1988,
112 1990] in a 2D-version as applied earlier to cold air outbreaks by *Lüpkes and Schlünzen*
113 [1996] and by *Birnbaum and Lüpkes* [2002] and to on-ice flow regimes by *Vihma et al.*

114 [2003]. Its 3D-version was applied to arctic regions by *Dierer and Schlünzen* [2005, 2005a]
115 and by *Hebbinghaus et al.* [2006]. The model is originally a mesoscale model with hor-
116 izontal grid spacing Δx of at least 1 km in convective conditions. However, we apply
117 it here with $\Delta x = 200$ m to resolve the integrated effect of convective plumes on the
118 ABL above leads. Since the typical scale of flow distortion due to leads is in the order of
119 kilometers, this phenomenon belongs to the microscale α , and we call the model in the
120 following a microscale model. It is non-eddy resolving, since populations of convective
121 eddies or individual plumes are not explicitly modelled, and their integral effect has to
122 be treated via the turbulence parameterization. Hence, the model differs strongly from
123 LES models with much smaller horizontal grid sizes, which are able to resolve convective
124 turbulence, i.e. dynamics of individual plumes. The METRAS version applied here is
125 based on the Boussinesq-approximated primitive equations with potential temperature
126 and three wind components as prognostic variables. We consider neither radiation nor
127 condensation processes while prescribing a dry atmosphere for simplicity.

128 The model equations are solved on a staggered ARAKAWA-C grid with 10 layers below
129 300 m and the first layer for temperature and horizontal wind at 10 m height. 34 layers
130 follow above this height, and the model top is at 8000 m, which allows the damping of
131 gravity waves towards the model top.

132 At lateral boundaries, boundary-normal gradients of boundary-parallel wind compo-
133 nents and of potential temperature are prescribed to zero. The boundary-normal wind is
134 derived from the prognostic momentum balance equations.

135 For initialization, the model requires the large scale geostrophic wind as well as quasi-
136 stationary profiles of potential temperature at the inflow boundaries. Such profiles are

137 determined with the 1D model version based on observed or prescribed meteorological
138 variables and profiles.

139 We neglect horizontal turbulent transport, since it was found from LES results that
140 in the relevant regions, influenced by convective plumes from leads, vertical turbulent
141 transports are much larger than the horizontal ones. Surface fluxes of heat and momentum
142 are calculated via Monin-Obukhov theory with similarity functions according to *Dyer*
143 [1974]. METRAS can be run with different closures for the calculation of turbulent fluxes
144 above the surface layer. However, the present application of the model requires a new
145 closure adjusted to the special conditions of a nonhomogeneous flow regime over leads.
146 The new closure will be derived in Section 5.

2.2. The LES Model

147 Besides METRAS, we use the **PA**rallelized **L**arge-eddy simulation **MO**del **PALM**
148 [*Raasch and Schröter*, 2001]. So far, PALM has been applied to study homogeneously
149 [*Schröter et al.*, 2000; *Gryanik et al.*, 2005] and heterogeneously heated convective bound-
150 ary layers (e.g., *Raasch and Harbusch* [2001]; *Letzel and Raasch* [2003]) as well as the
151 stably stratified boundary layer [*Beare et al.*, 2006]. A former non-parallelized version
152 has already been used by *Weinbrecht and Raasch* [2001] to study the flow above leads.
153 The model equations, the staggered grid, and the boundary conditions including stability
154 functions and roughness length are generally the same as in METRAS (see also next sub-
155 section). The subgrid-scale turbulence closure scheme is based on *Deardorff* [1980], using
156 an additional prognostic equation for the SGS turbulent kinetic energy.

157 The domain size is 40960 m \times 640 m \times 1472 m along x (lead orthogonal), y , and z .
158 The grid spacing is equidistant with 10 m along all directions except the vertical, where

159 it is smoothly stretched above 350 m. The first layer for temperature and the horizontal
160 wind components is at 5 m. Some cases were run also with increased resolution to test
161 the reliability of the coarse resolution runs.

162 As *Weinbrecht and Raasch* [2001] already showed, a high spatial resolution is required to
163 adequately resolve turbulent elements above the lead. For a lead width of 200 m and their
164 smallest grid spacing of 2 m, they failed to resolve the turbulence even for a comparably
165 small background wind of 5 m s^{-1} . As a compromise between resolution and CPU time
166 requirements, the ratio between lead width (1000 m) and grid spacing (10 m) in the present
167 study is just the same as in the *Weinbrecht and Raasch* study. Although our simulations
168 are therefore unable to resolve the very shallow convection above the first half of the lead,
169 the grid spacing should nevertheless be sufficient because *Weinbrecht and Raasch* [2001]
170 also found that the qualitative and quantitative structure of the downstream plume does
171 not significantly change for a smaller grid spacing.

172 The 1D temperature and wind profiles from METRAS are used for initialization. A
173 quasi-stationary state is reached after about 1800 s.

3. Scenarios and Setup of Models

174 In the present investigation we consider the flow across two leads of 1 km width and
175 10 km distance to each other. Such leads were often observed by *Lüpkes et al.* [2004] in
176 the Fram Strait region about 100 - 200 km north from the ice edge.

177 Ten cases were modelled, which differ in the geostrophic wind speed, near-surface ABL
178 temperature at the inflow boundary, and in the surface fluxes of sensible heat over the
179 leads. In all cases, which are summarized in Tables 1 and 2, the flow is approximately
180 orthogonal to the lead in the lowest 100 m. We distinguish between two sets of cases with

181 respect to the thermal situation. In the first one (cold cases) the surface temperature
182 and ABL temperature at the inflow position is prescribed to 250 K over pack ice. In the
183 second set (warm cases) the surface temperature of ice and ABL temperature amount to
184 260 K. The surface temperature of the lead is always assumed as 270 K, which is lower
185 than the freezing point, since often a layer of very thin ice or grease ice is developing
186 above newly formed leads.

187 In all cases, we assume a neutral boundary layer at the inflow boundary of the first lead,
188 which is capped by a strong inversion at 300 m height. Such a profile was observed by
189 aircraft during the campaign ARTIST [*Hartmann et al.*, 1999, *Wacker et al.*, 2005] over
190 the northern Fram Strait pack ice region. For simplicity and since our present focus is
191 on the investigation of the heat transport in higher levels, we decided to neglect the fetch
192 dependence of roughness (see introduction) and prescribe in both models the roughness
193 lengths for momentum to $z_0 = 10^{-3}$ m over pack ice and $z_0 = 10^{-4}$ m over the lead. The
194 roughness length for heat is assumed as one tenth of z_0 , which is also a simplification of
195 reality (see e.g., *Andreas and Murphy* [1986] and *Andreas and Cash* [1999]).

196 In both models the same lateral boundary conditions (zero gradient) and initial profiles
197 are used. However, the LES slightly modifies these profiles in the inflow region, since
198 it produces its own stationary solution and turbulence is too weak in the inflow region
199 (boundary about 10 km in front of the first lead) to be resolved by the LES. To trigger the
200 turbulence development the vertical velocity is disturbed randomly in the first kilometer
201 of the domain as in *Weinbrecht and Raasch* [2001]. Moreover, at the upstream side of the
202 second lead large eddies, generated over the first lead, naturally produce in our simulations
203 a well mixed ABL with turbulence being resolved by the LES. In other words, the first

204 lead plays the role of a natural trigger mechanism in our simulations, which is stronger
205 than the triggering by white noise. When we compare results of METRAS and of the LES
206 we concentrate, therefore, on the region over the second lead. We found that the impact
207 of differences between the inflow profiles of METRAS and of the LES at the upstream side
208 of the second lead on fluxes and temperatures are small compared with the lead impact.
209 For example, the maximum difference in temperatures is only 0.2 K, which can modify
210 the surface fluxes in the considered parameter range by 1-2 % only.

211 For simplicity, the models are run in their dry version with zero humidity. This is a
212 further simplification, but not too restrictive. During the cruise ARKTIS XIX/1 with RV
213 Polarstern in spring 2003 convection was observed very often over leads in the Barents
214 Sea and Fram Strait pack ice without the formation of clouds or sea smoke [*Lüpkes et al.*,
215 2004].

4. Results of the LES Model

216 In Figures 3 - 5 only those averaged fields of variables obtained with the LES are pre-
217 sented, which will later be compared with results of the microscale model. The averaging
218 period is 900 s as in *Weinbrecht and Raasch* [2001]. Spatial averaging is done parallel to
219 the lead (orthogonal to the incoming wind) across the entire domain.

220 Figures 3 and 4 show the potential temperature, the vertical turbulent fluxes of sensible
221 heat (sum of subgrid scale and resolved contribution) and the horizontal wind speed for
222 the weak-wind, medium-wind and strong-wind cases of the cold data sets (Table 1). In
223 all figures the inflow is directed from left to right and the lead position is from 0 to 1 km
224 distance. The topological structure of the quasi-stationary solutions seems to be similar in
225 all cases. There is a strong plume with upward fluxes in the order of 100 W m^{-2} in its core

(Figure 3). Obviously, the plumes penetrate slightly into the inversion while generating
turbulence and consequently an entrainment flux, which is visible in the figures by negative
(downward) fluxes on top of the plumes. One can distinguish well pronounced boundaries
of the plume separating the convection dominated regions from the environment. In the
weak-wind case the plume shape is more symmetric with respect to its centerline than in
the strong-wind case, where the turbulence is advected over a larger region downstream
of the lead than in the weak-wind case. Differences between the three cases are related
mainly to the inclination of the plume centerline and magnitude of surface heat fluxes.
The plume inclination increases with increasing wind and decreases with increasing surface
heat flux. The sensitivity to a variation of the wind speed is larger than to a variation of
the surface heat flux (see Table 1).

Within the most part of the modelled ABL the potential temperature increases slightly
with height. An unstable stratification (Figures 3 and 5) is found only in the plumes'
core.

Figures 3 and 5 illustrate that the vertical component of heat fluxes in the plume are
directed partly along the vertical temperature gradient (downgradient) and partly coun-
tergradient. The occurrence of countergradient fluxes is independent on the wind. In the
strong-wind case the region of countergradient fluxes occurs more on the downstream end
of the plume, whereas in the weak-wind case a more symmetric distribution of downgra-
dient and countergradient regions is found. In all cases the horizontal component of heat
fluxes (not shown) are small in and outside of the convective plume region.

Also the fields of horizontal wind have a similar topological structure in all cases (Figure
4). In the lowest 80 m the lead causes horizontal gradients in wind speed. However, wind

249 speeds vary only slightly in the layer between 80 m and 250 m. In all cases the vertical
250 velocity (not shown) turned out to be small (in the order of millimeters to centimeters
251 per second). This is due to the averaging in lead parallel direction, which cancels out the
252 effect of updrafts and downdrafts in the convective eddies.

253 The general flow features including the occurrence of countergradient fluxes are qualita-
254 tively similar to the results shown by *Glendenning and Burk* [1992] and by *Weinbrecht and*
255 *Raasch* [2001]. Quantitative differences can be attributed to the smaller lead width in the
256 latter studies and to differences in the meteorological conditions such as the prescribed
257 initial stratification.

5. Turbulence Closure for Microscale Modelling of Convection over Leads

5.1. Studies with Existing Closures

258 The LES results (Figure 5) clearly show the occurrence of countergradient heat fluxes.
259 It is well known (e.g., *Holtslag and Moeng* [1999], *Zilitinkevich et al.* [1999], *Van Dop*
260 *and Verver* [2001]) that such fluxes, which are independent on the local gradients of tem-
261 perature, can only be parameterized with a nonlocal closure. Nevertheless, we used the
262 microscale model in a first step with different local closures to clearly identify the draw-
263 backs. We applied a simple first order mixing length closure, summarized in Appendix A,
264 and closures based on the prediction of turbulent kinetic energy such as the 1.5th order
265 closure (level 2.5) of *Mellor and Yamada* [1974] and the closure of *Teixeira and Cheinet*
266 [2004]. The results of such model runs were all similar. There was a fair representation of
267 the wind field similar as that shown in Figure 7, but a temperature increase with height as
268 in the LES could never been obtained. Furthermore, the heat fluxes were either underes-
269 timated or - after tuning the maximum mixing length - the plume inclination became too

270 weak. It became obvious that an improvement of closures should account for the nature
 271 of nonlocal countergradient heat transport within the plumes.

272 The most simple closures allowing countergradient heat transport are those, which are
 273 based on the heat transport equation

$$\overline{w'\Theta'} = -K_H \left(\frac{\partial \overline{\Theta}}{\partial z} - \Gamma \right). \quad (1)$$

274 $\overline{w'\Theta'}$ is the turbulent heat flux and K_H is the eddy diffusivity for heat. Γ is sometimes
 275 called countergradient term, but this is misleading, since $K_H\Gamma$ is always an upward heat
 276 flux independent on the sign of the temperature gradient. Hence, we refer to $K_H\Gamma$ in the
 277 following as the nonlocal or nongradient flux and to $K_H(d\overline{\Theta}/dz)$ as the local or gradient
 278 flux.

279 There are several closures in literature using the above formulation. They differ mainly
 280 by the formulation of K_H and Γ . We tested the schemes of *Troen and Mahrt* [1986] and
 281 *Lüpkes and Schlünzen* [1996], henceforth abbreviated by LS96. The latter is used as a
 282 basis for a an improved closure for lead convection and is therefore described here in
 283 detail.

284 Equations for K_H and Γ of LS96 can be written in nondimensional form as a function of
 285 the stability parameter $S = w_*/u_*$, where u_* is the friction velocity and w_* the convective
 286 velocity scale [*Deardorff*, 1970] given by

$$w_* = \left(\frac{g}{\Theta_0} z_i \overline{w'\Theta'}|_s \right)^{1/3} = (B_s z_i)^{1/3}. \quad (2)$$

287 $B_s = (g/\Theta_0)\overline{w'\Theta'}|_s$ is the surface buoyancy flux, z_i is the mixed layer depth. We obtain
 288 (see Appendix B)

$$K_H/K_p = Z \left(1 + \frac{S}{\kappa} Z^{1/3}\right) (1 - Z)^2, \quad Z_p \leq Z \leq 1 \quad (3)$$

289 with the nondimensional vertical coordinate $Z = z/z_i$ and the eddy diffusivity at the
 290 surface layer top z_p

$$K_p = u_* \kappa z_p / \Phi_p \quad (4)$$

291 with $\Phi_p = (\Phi_H|_{z_p} + \Phi_\Gamma) Z_p (1 + (S/\kappa) Z_p^{1/3}) (1 - Z_p)^2$. Φ_H is the Monin Obukhov similarity
 292 function for heat and $\Phi_\Gamma = \Gamma|_{z_p} \kappa z_p u_* / \overline{w'\Theta'}|_s$. Due to the above K_H -formulation, a
 293 matching of heat fluxes with surface layer fluxes is achieved, which guarantees continuity
 294 of fluxes with height at z_p .

295 The nonlocal term Γ is parameterized as

$$\Gamma/\Gamma_0 = 0.63 b S \left[(1 - Z)^{3/2} + 0.593 S^3 Z (1 - 0.9Z)^{3/2} \right]^{-2/3}, \quad (5)$$

296 where $\Gamma_0 = (\overline{w'\Theta'}|_s)/(u_* z_i)$. In equations (3), (4), and (5) the stability parameter S
 297 represents the relative importance of convective and mechanical mixing.

298 It is important to note that with equations (3) - (5) the forcing of turbulence is related
 299 at any position with coordinates (y, z) to the properties of the surface at location $(y, 0)$,
 300 where y and z are the horizontal and vertical coordinates, respectively. Thus, application
 301 of the nonmodified LS96 scheme to the microscale model simulating the flow over leads
 302 restricts the plume region to the lead region and generates a non-inclined plume, since

303 downstream of the lead the surface heat flux is close to zero or even negative. This is in
 304 large contrast to the LES results showing an inclined plume.

5.2. A new closure

305 5.2.1. Principles

306 Motivated by the above results with existing closures a new closure was developed,
 307 which is based on the following principles:

308 1. Heat transport in convective plumes originating from a lead (grey shaded in Figure
 309 2) is dominated by nonlocal effects, while farer away from the plumes mixing is local.
 310 As the basic scheme in the convective core region, we use the closure by LS96, which is
 311 adopted to the nonhomogeneous conditions. At the boundaries of the plume, we switch
 312 to a local closure (in this paper to that described in Appendix A).

313 2. The switching lines are given by the local heights of the internal boundary layers
 314 $\delta(y)$ (upper plume boundary) and $\delta_d(y)$ (lower plume boundary) with $y =$ distance from
 315 the lead's upstream edge.

316 3. The functional forms of the vertical profiles of the eddy diffusivity for heat K_H and
 317 of the nonlocal term Γ at each position above and downstream of the lead remain the
 318 same as over a homogeneous surface, but K_H and Γ are scaled with the fetch dependent
 319 $\delta(y)$ instead of z_i . The fetch dependence of K_H and Γ is accounted for by introducing a
 320 fetch dependence of the stability parameter $S = S(y)$.

321 4. Dominating parameters for the processes in the convective core region above and
 322 downstream of the lead are: the surface buoyancy flux over the lead $B_l = g/\Theta_0 \overline{w'\Theta'}|_l$,
 323 the vertically integrated mean horizontal velocity at the lead's upstream edge U , and the
 324 inversion layer height z_i .

325 5. We consider in the present paper only cases with neutral stratification in a shallow
 326 ABL capped by an inversion strong enough to avoid convection from penetrating a long
 327 distance into the inversion layer. Hence, stratification within the shallow ABL does not
 328 appear as parameter, and we prescribe z_i as constant.

329 6. Momentum fluxes are determined with a local closure (Appendix A), which is applied
 330 to the entire domain.

331 5.2.2. Internal Boundary Layer Heights and Stability Parameter

332 To realize the above principles for the nonlocal closure and its matching with the local
 333 one, the stability parameter S and the internal boundary layer height δ should be spec-
 334 ified as functions of y . The largest difficulty in defining S and δ consists in the correct
 335 introduction of the characteristic vertical velocity scale, which occurs in both S and δ .

336 Our approach is as follows. For $0 < y < L$, the velocity of the convective eddies
 337 may be taken as equal to the same velocity as used in homogeneous conditions, namely
 338 $w_l = (B_l \delta)^{1/3}$, where we use subscript l instead of asterisk $*$ to avoid confusion with the
 339 Deardorff scale w_* (Equation 2). This scale is reasonable, because the largest eddies have
 340 a horizontal scale smaller than 2δ and $2\delta < L$, thus the assumption of homogeneity can be
 341 used in that region. However, for $y > L$, due to lateral entrainment and dissipation, the
 342 characteristic convective velocity is reduced in comparison with w_l in the region $0 < y < L$.
 343 We express this reduction by an exponential decay function and take the characteristic
 344 convective velocity scale as

$$w_l(y) = c (B_l \delta)^{1/3} \exp(-(y/D)) , \quad (6)$$

345 where D is the decay length scale to be specified below. c is an adjustable constant. We
 346 can use equation (6) in the full range $y > 0$ for small leads.

347 δ and the decay length scale D are derived as follows. We assume that the local
 348 inclination angle of the plume boundary $\phi \approx tg(\phi) \approx d\delta/dy$ is equal to $w_e/(U + u_e)$,
 349 where U is the mean horizontal velocity at the upper plume boundary and w_e and u_e are
 350 the entrainment vertical and horizontal velocity at the same boundary. Furthermore, in
 351 the range of parameters studied $u_e \ll U$ in accordance with LES data (not shown). Thus,
 352 the internal boundary layer equation (see also *Monin and Yaglom* [1971]; *Turner* [1986])
 353 reads

$$\frac{d\delta}{dy} = \frac{w_e(y)}{U}. \quad (7)$$

354 Furthermore, we assume that δ is influenced by the strongest convective eddies in the
 355 plume, whose vertical velocity is w_{max} . Thus, we can write $w_e = a_e w_{max}$, where a_e
 356 is constant. Finally, we use the assumption that w_{max} is scaled with the characteristic
 357 convective velocity (6) as $w_{max} = a_m w_l$, where a_m is also an adjustable constant. After
 358 expressing now w_e in terms of w_l , using (6) in (7), and integration with the boundary
 359 condition $\delta = 0$ for $y = 0$, we obtain

$$\delta(y) = \delta_{max} (1 - \exp(-y/D))^{3/2} \quad (8)$$

360 with the plume penetration height

$$\delta_{max} = \left(\frac{2a}{3} \frac{B^{1/3} D}{U} \right)^{3/2}, \quad (9)$$

361 where $a = a_e c a_m$. Since in a neutral environment convective turbulence always pene-
 362 trates up to the inversion, we can set $\delta_{max} = z_i$ in equation (9). We find then the decay
 363 length scale as

$$D = \frac{3}{2a} \left(\frac{U^3}{B_l} \right)^{1/3} z_i^{2/3}. \quad (10)$$

The length scale D has a simple physical meaning: $D \approx U\tau$, where $\tau \approx z_i/w_* \approx z_i^{2/3}/B_l^{1/3}$ is the eddy turnover time of the largest available convective eddies in the plume. Finally, with the constraint of maximal penetration $\delta_{max} = z_i$, equation (8) reads

$$\delta(y) = z_i (1 - \exp(-y/D))^{3/2} \quad (11)$$

364 with D given by equation (10). Due to equation (11) $\delta(y)$ is independent from z_i , if
 365 $y \ll D$, namely $\delta(y) \approx z_i(y/D)^{3/2} = (2a/3)^{3/2}(B_l^{1/2}/U^{3/2})y^{3/2}$. Furthermore, $\delta(y) \approx z_i$, if
 366 $y \gg D$.

As mentioned above, we match the nonlocal closure with the local closure downstream of the plume. We introduce the downstream lower boundary of the plume $\delta_d(y)$ by the constraint

$$\overline{w'\Theta'}_{ng}|_{z=\delta_d} = K_H \Gamma|_{z=\delta_d} = \overline{w'\Theta'}_{crit}, \quad (12)$$

367 where $\rho c_p \overline{w'\Theta'}_{crit} = F_{crit}$ is some threshold value close to zero. This definition of the plume
 368 boundary is based on the analysis of LES data showing that heat fluxes are predominantly
 369 non gradient fluxes at the lower plume boundary δ_d (Figure 5).

370 It is possible to give an a priori estimation of the constants a and c . First, constant c
 371 can be estimated as $c \approx 1.6 \pm 0.5$ (see Appendix C). This is based on the assumption that
 372 in the core of the plume convective turbulence is fully developed and similar to convective

373 turbulence over homogeneous surfaces. The constant a_e characterizes the entrainment
 374 and is in the range 0.2-0.4 (see *Turner*, 1986). The constant a_m depends on the shape of
 375 the vertical velocity profile in the plume, and it is between 2 and 4 for reasonable profiles.
 376 Thus, $a = a_e c a_m$ is defined by three different processes and is in the range between 0.4
 377 and 3.4. It can be expected that the critical heat flux F_{crit} is a few percent only of the
 378 surface flux over the lead.

379 5.2.3. Parameterization in the Convective Region

380 To arrive at the equations of the new parameterizations, one has simply to replace z_i
 381 in the equations of the LS96 closure (section 5.1) by $\delta(y)$. The surface heat flux and the
 382 friction velocity occurring in these equations represent now average values above the lead
 383 surface. The new scheme consists then of equations (1) and (3) - (6), with $Z = z/\delta(y)$
 384 and with $S = w_l(y)/u_{*,l}$, where index l refers to the lead surface. $\delta(y)$ is given by equation
 385 (11) and $\delta_d(y)$ is defined by equation (12). Practically, equation (12) does not have to be
 386 solved for δ_d , but when the non-gradient heat flux is lower than F_{crit} the local closure has
 387 to be used.

388 The closure in the convective region depends on three constants, b in equation (5), c
 389 in equation (6), and a in equation (10). The possible range of values for these constants
 390 has been estimated above. To confirm and optimize these values, at first the weak-wind,
 391 medium-wind, and strong-wind cases of the cold situation were modelled (Table 1). The
 392 constants were determined as $a = 2.3$, $b = 0.6$, $c = 1.6$. Note that the value for c is
 393 equivalent to its value estimated before in Section 5.2.2. Hereafter, it was shown that
 394 the optimum values for these reference cases are still valid in the remaining seven cases

395 covering the parameter range, for which the parameterization has been derived. F_{crit} was
396 determined as 2 W m^{-2} for all cases.

397 5.2.4. Matching With the Surface Layer and With the Local Closure

398 In the region outside of the plume the local closure is used as described in Appendix
399 A. The plume boundaries are defined by δ and δ_d . At the upper boundary the eddy
400 diffusivities for heat, and hence, the heat fluxes go to zero. The latter behaviour is
401 approximately achieved also at the lower boundary by use of the decay function. Since we
402 consider convection in a neutral or slightly stable environment, heat fluxes are also small
403 or zero outside the plume, where the local closure is applied. Thus, an implicit matching
404 is obtained.

405 At the lead surface ($0 < y < L$) the heat fluxes match with the surface fluxes obtained
406 from Monin Obukhov theory, since this property of the parameterization is already pre-
407 scribed in the LS96 closure.

6. Results of the Microscale Model Obtained With the New Closure

6.1. Cold Cases

408 In Figures 6 and 7 results of the three reference runs (weak-wind, medium-wind, strong-
409 wind) are presented, which were obtained with the closure as described in the previous
410 section using equations (1) and (3) - (6) and with constants a , b , c , set to the optimum
411 values 2.3, 0.6, and 1.6 as mentioned above. According to the figures, the overall structures
412 of the modelled fields agree well with those of the LES solution. As in the LES results
413 the potential temperature increases with height downstream of the lead and an unstable
414 stratification occurs only in a small region in the plume's core. The inclination of the

415 plumes marked by upward heat fluxes agrees well with the LES results in all cases. The
416 inclination angle decreases with increasing wind speed as in the LES. Also the amount of
417 fluxes is well reproduced (Table 1). In the reference runs, the deviation of the maximum
418 fluxes at 200 m and 100 m between both models is in the order of 10 % with a general
419 underestimation of fluxes at 100 m. However, this points more to a slight problem with
420 the LES rather than to a failure of the parameterization. Close to the surface, the LES
421 cannot resolve convection within the first 100 m distance over the lead. This results in an
422 unrealistic peak in the fluxes further downstream, which is still slightly visible at 100 m
423 height. A further investigation with increased LES resolution showed indeed a weakening
424 of near-surface heat flux maxima.

425 In Figure 5, the regions with fluxes along the gradient and counter to the gradient are
426 shown, which result from the microscale model with the new closure. These regions agree
427 fairly well with the corresponding LES results shown in the same figure.

428 Two further cold cases were considered. In case 2 (Table 1) the quality of agreement
429 between the microscale model and LES results is similar as in the reference cases. Only
430 in case 5, which is the case with the strongest wind, fluxes are strongly overestimated
431 by METRAS at 200 m height. However, as already described by Weinbrecht and Raasch
432 (2001), this might also be a sign that the LES resolution for the strongest wind should be
433 better than the used one.

6.2. Warm Cases

434 In Figures 8 and 9 results are presented for the same forcing wind speeds as in the cold
435 cases, but now for significantly warmer conditions (see also Table 2). Heat fluxes over the
436 lead amount now to less than 50 % of the values in the cold cases. The plume inclination

437 angles decrease in comparison with the cold cases. This result can be expected, since
438 the characteristic convective velocity w_l decreases with decreasing heat fluxes over the
439 lead. The quality of agreement remains approximately the same as in the cold cases. This
440 concerns the absolute values of fluxes, the inclination of the plumes, and the topology of
441 the temperature distribution. But in the weak-wind case the increase of temperature with
442 height is slightly overestimated by the microscale model. It should be emphasized that
443 the same set of constants has been used as in the cold cases. The sensitivity on different
444 values of these constants is described in the following for some of the cold cases.

6.3. Sensitivity Studies

445 To test the sensitivity on the nonlocal fluxes, we used the new closure with different
446 values of the proportionality constant b in equation (5). According to the results for the
447 medium-wind case, shown in Figure 10, b can be increased by 50 % without a change
448 of the qualitative structure of results, but an increase of b causes a stronger increase of
449 temperature with height. This is due to the redistribution of heat in the ABL from lower
450 levels to higher levels. Hence, an increase of b results in lower temperatures close to the
451 surface and in higher values in the upper third of the ABL.

452 The sensitivity of the model results was also tested on the inclination of the plume by
453 a variation of parameter a (equation 7). Furthermore, different values were used for c ,
454 the parameter occurring in the decay function (6). Typical results are shown in Figures
455 11 and 12. A strong variation of c by about ± 25 % modifies the fluxes only slightly.
456 The stability downstream of the lead increases with increasing c . A modification of a by
457 ± 15 % has a moderate effect on both fluxes and temperature. Fluxes at 100 m height
458 increase by about 10 %, when a is altered from 2.0 to 2.6 (medium-wind case).

459 We found, furthermore, that there is only a weak sensitivity of the results to the thresh-
460 old value of the nongradient heat flux F_{crit} (equation (12)) introduced to separate the
461 plume region from the outer region. An effect of a modified value was visible in the wind
462 fields, where the modelled peak above the lead was less pronounced, when we increased
463 the plume region considerably by reducing F_{crit} from its value 2 W m^{-2} used for the runs
464 shown in the figures to a value close to zero.

465 Obviously, the structure of model results is very robust against changes of constants.
466 The largest sensitivity is on b , whereas the sensitivity to variations of a , c and of F_{crit} is
467 small.

468 We tested also the sensitivity of the results on different formulations of the nonlocal
469 term Γ . E.g., we used the *Troen and Mahrt* [1986] formulation of Γ , first together with
470 the present eddy diffusivity (Equation 3). We obtained the same qualitative structure of
471 results, but it was not possible to get the same good agreement with the LES results in
472 all wind cases using only one set of constants. An optimal choice of constants for the
473 strong-wind case led to a strong overestimation of the stratification for the weak-wind
474 case. Finally, we tried to apply the complete scheme of *Troen and Mahrt* [1986] including
475 their eddy diffusivity with appropriate modifications as in section 5.2 for the LS96 scheme.
476 This did not work, however, and this failure could be traced back to the too low values
477 for the eddy diffusivity of heat, which resulted from such a modified Troen and Mahrt
478 closure. This is in contrast to an application of the scheme in homogeneous convective
479 conditions. LS96 showed that in such conditions the lower eddy diffusivities, and hence,
480 the lower local fluxes in the Troen and Mahrt scheme could be compensated by a larger
481 nonlocal flux.

6.4. Nonlocal Momentum Transport

482 The LS96 closure for convection above homogeneous regions and that of *Troen and*
483 *Mahrt* [1986] contain a nonlocal parameterization of the eddy diffusivity for momentum.
484 In the schemes of *Frech and Mahrt* [1995] and of *Noh et al* [2003] countergradient fluxes of
485 momentum fluxes are considered. We tested the new closure also with a parameterization
486 of the nonlocal momentum transport similar as in the LS96 closure (results not shown).
487 However, our results of the present scheme indicate that the wind fields agreed slightly
488 better with LES results, when the nonlocal closure for heat transport was combined with
489 the local closure of Appendix A for the parameterization of momentum fluxes.

6.5. Remarks on the Region of Applicability

490 We developed and tested the closure up to now only for a limited range of parameters,
491 for which LES runs were available. Hence, the application of the closure including the
492 specification of constants c , b , and a is restricted to the tested range ($L = 1$ km, $z_i = 300$ m,
493 $3 \text{ ms}^{-1} < U < 10 \text{ ms}^{-1}$, $51 \text{ Wm}^{-2} < F_s < 270 \text{ Wm}^{-2}$). In this range the present
494 parameterization does not use the width of the lead L as an external parameter. A future
495 development of the scheme should account for variable lead widths, which would result
496 probably in a specification of the constants in terms of the nondimensional parameters
497 L/z_i and L/D . But this needs a thorough analysis of appropriate LES results for larger
498 leads and smaller ABL heights.

499 The assumption of small inclination angles for the plume's centerline, used in equation
500 (8) is also crucial for our parameterization. This assumption means that $w_e \ll (U + u_e)$,
501 which is valid for nonzero wind with $U \gg u_e$. In the opposite limiting case of zero or
502 very low winds the investigation of *Esau* [2007] indicates that $u_e \approx w_e$, which means that

503 horizontal entrainment is as important as vertical entrainment. In our case, horizontal
504 advection dominates the horizontal entrainment.

505 The validity of the closure is also restricted to cases without recirculation effects of
506 the flow as obtained by *Mauritsen et al.* [2005] and which can develop in case of very
507 weak wind and strong fluxes. Furthermore, we consider only cases without an interaction
508 of plumes from different leads. This means that D should be smaller than the distance
509 between leads.

7. Summary and Conclusions

510 In this paper we studied the effect of leads on the arctic ABL. To this end we carried out
511 LES, developed a new scaling and parameterization based on this, and finally implemented
512 it to a meso/microscale model. Our studies had two main goals. The first was to model
513 an idealized scenario of the flow above leads in the arctic pack ice with an LES model
514 for winter or springtime meteorological conditions. These are characterized in the Fram
515 Strait region often by a close to neutral ABL over pack ice with a strong capping inversion
516 and by large temperature differences between the near-surface air and the lead surface.
517 The second goal was to model the same situation with a microscale model being able
518 to resolve the integrated effect of the developing plumes above leads rather than the
519 individual plumes. This is a non-trivial task, since classical turbulence closures are not
520 developed for regions with strong discontinuous thermal surface inhomogeneities and sharp
521 transition zones from convectively to mechanically dominated flow regimes. Hence, it
522 became necessary to develop a new closure for microscale modelling of the flow over leads.

523 The LES runs led to the result that the strong convective non-gradient heat transport
524 from leads has a stabilizing effect on the ABL downstream of leads. This increase of

525 potential temperature can only be obtained with a non eddy resolving model by using
526 a nonlocal closure for heat transport. Furthermore, such a closure should account for
527 the internal boundary layers developing downstream of leads. Eddy diffusivities and
528 nongradient fluxes should depend on the distance y to the lead. We developed a new
529 scaling by introducing the y -dependent internal boundary layer height and characteristic
530 vertical velocity for the plume region and used it for the development of a new closure,
531 which is based on the nonlocal closure of LS96 in the plume regions. Outside this region a
532 local closure was applied. With this new unified local plus nonlocal closure it was possible
533 to simulate the mean wind field, temperatures, and heat fluxes in the close environment
534 of leads.

535 The new closure contains three open constants. We adjusted them using three model
536 runs from the LES. It turned out that one of the constants agreed well with its value
537 estimated from theory. We found then that the same set of constants was working for
538 other cases with different wind and temperature conditions as well. The topology of
539 wind, temperature and fluxes characterized e.g., by the plume inclination and regions with
540 increase and decrease of potential temperature with height could be well reproduced. Also
541 the absolute values of fluxes were not too far from the LES. The generally good agreement
542 of modelled fluxes and temperatures obtained with the new closure can be explained by
543 the correct parameterization of relative contributions of gradient and countergradient
544 transport due to small scale and large scale convective eddies, respectively.

545 Sensitivity studies showed that the new parameterization is rather robust against modifi-
546 cations of the constants, since at least the overall structure of the modelled fields remained
547 unchanged, when the constants were changed moderately.

548 Despite the good agreement between the results of the microscale and the LES model,
 549 we would like to stress that the present scheme is limited to a restricted range of parame-
 550 ters. Up to now, we considered ten cases, differing considerably by the wind, temperature
 551 and by the surface fluxes. But the sensitivity on wind direction, on a variation of z_i , on
 552 the stability in the background ABL, and on the lead width was not investigated. We
 553 expect that especially in case of larger lead widths, low wind speeds, and stable inflow
 554 conditions modifications of the scheme will become necessary in the future. Probably, the
 555 constants of the parameterizations have to be specified then in terms of the nondimen-
 556 sional parameters L/z_i and L/D (see Section 6.5). In the present study we concentrated
 557 on the impact of single leads. In the future, the microscale model could be applied at
 558 low computational costs to a domain being representative for one grid cell of a large scale
 559 model to study the integral effect of a series of leads on ABL processes dependent on the
 560 external forcing. Thus, the present study represents an important first step towards the
 561 future derivation of a more general parameterization of the lead impact on ABL processes,
 562 which could be used then in climate and weather prediction models.

563

564 **Appendix A, Local Mixing Length Closure**

565 The present local closure is described by *Herbert and Kramm* [1985] as well as *Kramm*
 566 [1995] with the eddy diffusivities for heat K_H and momentum K_M depending on the
 567 stability corrected mixing length l_n

$$K_M = \begin{cases} l_n^2 \left| \frac{\partial v}{\partial z} \right| (1 - 5Ri)^2 & , 0 \leq Ri \leq Ri_c \\ l_n^2 \left| \frac{\partial v}{\partial z} \right| (1 - 16Ri)^{1/2} & , Ri \leq 0 \end{cases} \quad (\text{A1})$$

568 and

$$K_H = \begin{cases} K_M & , 0 \leq Ri \leq Ri_c \\ K_M (1 - 16Ri)^{1/4} & , Ri \leq 0 \end{cases} \quad (\text{A2})$$

569 where $Ri_c = 0.2$ is the critical Richardson number and l_n the mixing length for neutral
570 stratification. The latter is specified according to *Blackadar* [1962] as

$$l_n = \frac{\kappa z}{1 + \frac{\kappa z}{l_{max}}} \quad (\text{A3})$$

571 $\kappa = 0.4$ is the v. Karman constant. Based on studies of *Brown* [1996] we parameterize
572 l_{max} as 15 % of the ABL height z_i . *Vihma et al.* [2003] have shown that this closure
573 produced fluxes very close to observed values in the case of on-ice flow with a shallow
574 neutral and stable ABL above sea ice. A comparable quality of results was obtained by
575 *Vihma et al.* [2005] with a similar closure in case of weak convection above sea ice due to
576 cold air advection.

577 Different from many other local closures, which depend also on the Richardson number,
578 the above formulation of eddy diffusivities guarantees matching of fluxes at the top of
579 the surface layer (first grid level) with surface layer theory, when similarity functions of
580 *Dyer* [1974] are used in the surface layer. In the original formulation equations (A1) and
581 (A2) are restricted to $Ri > -5$, in case of smaller Richardson numbers, originally a free
582 convection parameterization is proposed. We applied the above formulation, however,
583 also for $Ri < -5$ to circumvent unsolved problems of matching the closures for different
584 regimes of Ri .

585

586 **Appendix B, Reformulation of the LS96 Closure**

587 The LS96 closure uses the heat transport equation (1) with the eddy diffusivity

$$K_H = \frac{\kappa u_* z_p}{(\Phi_H - \kappa z_p / \Theta_* \Gamma|_{z_p})} \left(\frac{z_i - z}{z_i - z_p} \right)^2 \frac{u_* \kappa z + w_* z_i (z/z_i)^{4/3}}{u_* \kappa z_p + w_* z_i (z_p/z_i)^{4/3}}, \quad (z_i \geq z \geq z_p), \quad (\text{B1})$$

588 where u_* is the friction velocity and Θ_* the characteristic surface layer temperature
 589 scale. This formulation was derived on the basis of a K_H -parameterization by *Holtslag*
 590 *and Moeng* [1991]. In contrast to their formulation, it accounts for both mechanical and
 591 convective mixing by the terms proportional to u_* and to w_* , respectively, and guarantees
 592 matching of heat fluxes between the main part of the ABL and the surface layer fluxes
 593 obtained from Monin Obukhov theory.

In LS96, the nonlocal term Γ is parameterized following *Holtslag and Moeng* [1991] as

$$\Gamma = b \frac{w_* \overline{w'\Theta'}|_s}{w'^2 z_i}, \quad (\text{B2})$$

where b is a proportionality constant. b was set to 2 by *Holtslag and Moeng* [1991], but
 LS96 obtained a better agreement with observations using $b = 3$. The variance of the
 vertical velocity $\overline{w'^2}$ is approximated in equation (B2) by

$$(\overline{w'^2})^{3/2} = 1.6^{3/2} u_*^3 \left(1 - \frac{z}{z_i}\right)^{3/2} + 1.2 w_*^3 \left(\frac{z}{z_i}\right) \left(1 - 0.9 \frac{z}{z_i}\right)^{3/2}. \quad (\text{B3})$$

594 Using nondimensionalization with $z = z_i Z$, and introducing the nondimensional stabil-
 595 ity parameter $S = w_*/u_*$ in the above equations leads to

$$\overline{w'^2} = 1.6 u_*^2 \left[(1 - Z)^{3/2} + \frac{1.2}{1.6^{3/2}} S^3 Z (1 - 0.9Z)^{3/2} \right]^{2/3} \quad (\text{B4})$$

596 After substituting equation (B4) in equation (B2), and using again the nondimension-
 597 alization, it is straightforward to obtain equations (3) - (5). The constants 1/1.6 and
 598 1.2/1.6^{3/2} have been calculated as 0.63 and 0.593, respectively.

599

600 **Appendix C, Theoretical Determination of the Constant c**

601 Substituting equation (11) into (6), we can find $w_l(y)$ as an explicit function of y :

$$w_l(y) = c w_* \left[1 - \exp(-y/D) \right]^{1/2} \exp(-y/D), \quad (\text{C1})$$

602 where w_* is the Deardorff velocity scale (equation 2). $w_l(y)$ is a nonmonotonic function,
603 which approaches to zero at $y = 0$ and $y \rightarrow \infty$. Its maximum is

$$\max(w_l) = c \frac{2}{3\sqrt{3}} w_* \approx 0.38 c w_*. \quad (\text{C2})$$

604 At the same time, we can also calculate the maximum of the characteristic vertical velocity
605 for convection in homogeneous conditions as $\max(\sqrt{w'^2})$. Using the convective part in
606 equation (B3), we find

$$\max\sqrt{(w'^2)} = (1.2)^{1/3} (4/9)^{1/3} (3/5)^{1/2} w_* \approx 0.63 w_*. \quad (\text{C3})$$

607 Assuming that in the core of the plume convection is fully developed and that it is similar
608 to homogeneous conditions, we can assume that $\max(w_l) = \max\sqrt{(w'^2)}$. Hence, we obtain
609 the estimation $c \approx 1.6$. We expect that this simple estimation, which neglects e.g., the
610 mechanical part of the w -variance, is reasonable with 30 % accuracy.

611 **Acknowledgments.** We thank the associated editor and one of the referees for help-
612 ful comments and suggestions. This study was supported by the EU project DAMO-
613 CLES, which is financed in the 6th Framework Programme for Research and Develop-
614 ment (grant 18509) and by DFG (grant no. LU 818/1-1). The LES runs were performed

615 on an IBM pSeries 690 supercomputer of the Norddeutscher Verbund für Hoch- und
616 Höchstleistungsrechnern (HLRN).

References

- 617 Alam, A., and J. A. Curry (1997), Determination of surface turbulent fluxes over leads in
618 arctic sea ice, *J. Geophys. Res.*, *102*, 3331–3344.
- 619 Andreas, E. L., Paulson, C. A., Williams, R. M., Lindsay, R. W., and J.A. Businger (1979),
620 The turbulent heat flux from arctic leads, *Boundary-Layer Meteorol.*, *17*, 57–91.
- 621 Andreas, E. L., and B. Murphy (1986), Bulk transfer coefficients for heat and momentum
622 over leads and polynyas, *J. Phys. Oceanogr.*, *16*, 1875–1883.
- 623 Andreas, E. L., and B. A. Cash (1999), Convective heat transfer over wintertime leads
624 and polynyas, *J. Geophys. Res.*, *104 (C11)*, 25,721–25,734.
- 625 Beare, R. J., Cortes, M. A. J., Cuxart, J., Esau, I., Golaz, C., Holtslag, A. A. M., Khairout-
626 dinov, M., Kosovic, B., Lewellen, D., Lund, T., Lundquist, J., McCabe, A., Macvean,
627 M. K., Moene, A., Noh, Y., Poulos, G., Raasch, S. and P. Sullivan (2006), An Inter-
628 comparison of Large-Eddy Simulations of the Stable Boundary Layer, *Boundary-Layer*
629 *Meteorol.*, *118*, 247–272.
- 630 Birnbaum, G., and C. Lüpkes (2002), A new parameterisation of surface drag in the
631 marginal sea ice zone, *Tellus A*, *54A(1)*, 107–123.
- 632 Blackadar, A. K. (1962), The vertical distribution of wind and turbulent exchange in a
633 neutral atmosphere, *J. Geophys. Res.*, *67*,3095–3102.
- 634 Brown, A. R. (1996), Evaluation of parameterization schemes for the convective boundary
635 layer using large-eddy simulation results, *Boundary-Layer Meteorol.*, *81*, 167–200.

- 636 Deardorff, J. W. (1970), Convective velocity and temperature scales for the unstable
637 planetary boundary layer and for Rayleigh convection, *J. Atmos. Sci.*, *27*, 1211–1213.
- 638 Deardorff, J. W. (1980), Stratocumulus-capped mixed layers derived from a three-
639 dimensional model, *Boundary-Layer Meteorol.*, *18*, 495–527.
- 640 Dierer, S., and K.H. Schlünzen (2005), Atmosphere-sea ice interactions during cyclone
641 passage investigated by using model simulations and measurements, *Month. Wea. Rev.*,
642 *133*, No.12, 3678–3692.
- 643 Dierer, S., and K.H. Schlünzen (2005a), Influence parameters for a polar mesocyclone
644 development, *Meteorol. Zeitschrift*, *14*, 781–792.
- 645 Dyer, A. J. (1974), A review of flux-profile relationship, *Boundary-Layer Meteorol.*, *7*,
646 363–372.
- 647 Ertel, H. (1942), Der vertikale Turbulenz-Wärmestrom in der Atmosphäre, *Meteor. Z.*,
648 *59*, 250–253.
- 649 Esau, I.N. (2007), Amplification of turbulent exchange over wide arctic leads: Large-eddy
650 simulation study, *J. Geophys. Res.*, *112*, D08109, doi:10.1029/2006JD007225.
- 651 Frech, M., and L. Mahrt (1995), A two-scale mixing formulation for the atmospheric
652 boundary layer, *Boundary-Layer Meteorology*, *73*, no. 1-2, 91–104.
- 653 Glendening, J.W., and S.D. Burk (1992), Turbulent transport from an arctic lead: A large
654 eddy simulation, *Boundary-Layer Meteorol.*, *59*, 315–339.
- 655 Gryanik, V.M., Hartmann, J., Raasch, S., and M. Schröter (2005), A refinement of the
656 Millionshchikov quasi-normality hypothesis for convective boundary layer turbulence,
657 *J. Atmos. Sci.*, *62*, 2632–2638.

- 658 Hartmann, J., Albers, F., Argentini, S., Bochert, A., Bonafe, U., Cohrs, W., Conidi,
659 A., Freese, D., Georgiadis, T., Ippoliti, A., Kaleschke, L., Lüpkes, C., Maixner, U.,
660 Mastrantonio, G., Ravegnani, F., Reuter, A., Trivellone, G., and A. Viola (1999), Arctic
661 Radiation and Turbulence Interaction Study (ARTIST), *Reports on Polar Research,*
662 *Alfred Wegener Institute for Polar and Marine Research, Bremerhaven, 305*, 81 pp.
- 663 Hebbinghaus H., Dierer S., and K. H. Schlünzen K.H. (2006), Sensitivity studies on vortex
664 development over a polynya, *Theoretical and Applied Climatology*, DOI 10.1007/s00704-
665 006-0233-9.
- 666 Herbert, F., and G. Kramm (1985), Trockene Deposition reaktionsträger Substanzen,
667 beschrieben mit einem diagnostischen Modell der bodennahen Luftschicht, Published in:
668 Becker, K.H. and J. Löbel (Edts.): *Atmosphärische Spurenstoffe und ihr physikalisch-*
669 *chemisches Verhalten.*, Springer Verlag, Berlin, 264 pp.
- 670 Holtslag, A .A. M., and C. H. Moeng (1991), Eddy Diffusivity and countergradient trans-
671 port in the convective atmospheric boundary layer, *J. Atmos. Sci.*, *48*, 1690–1698.
- 672 Kramm, G. (1995), Zum Austausch von Ozon und reaktiven Stickstoffverbindungen zwis-
673 chen Atmosphäre und Biosphäre, *Schriftenreihe Fraunhofer Institut für Atmosphärische*
674 *Umweltforschung, Bd. 34*, ISBN 3-927548-75-8, 268 pp.
- 675 Letzel, M. O., and S. Raasch (2003), Large-eddy simulation of thermally induced oscilla-
676 tions in the convective boundary layer, *J. Atmos. Sci.*, *60*, 2328–2341.
- 677 Lüpkes, C., and K. H. Schlünzen (1996), Modelling the arctic convective boundary-layer
678 with different turbulence parameterisations, *Boundary-Layer Meteorol.*, *79*, 107–130.
- 679 Lüpkes, C., Hartmann, J., Birnbaum, G., Cohrs, W., Yelland, M., Pascal, R., Spiess,
680 T., and M. Buschmann (2004), Convection over arctic leads (COAL), Published in

- 681 Schauer, U. and G. Kattner (Edts.): *The expedition ARKTIS XIX/1 a,b and XIX/2*
682 *of the Research Vessel Polarstern in 2003, Reports on Polar Research, Alfred Wegener*
683 *Institute for Polar and Marine Research, Bremerhaven, 481, 47–62.*
- 684 Lüpkes, C., Vihma, T., Birnbaum, G., and U. Wacker (2008), Influence of leads in sea
685 ice on the temperature of the atmospheric boundary layer during polar night, *Geophys.*
686 *Res. Lett.*, *35*, L03805, doi:10.1029/2007GL032461.
- 687 Mauritsen T., Svensson, G., and B. Grisogono (2005), Wave flow simulations over arctic
688 leads, *Boundary-Layer Meteorology*, *117*, 259–273.
- 689 Mellor, G.L., T. and Yamada (1974), A hierarchy of turbulence closure models for plane-
690 tary boundary layers, *J. Atmos. Sci.*, *31*, 1791–1806.
- 691 Monin, A. S., and A. M. Yaglom (1971), *Statistical Fluid Mechanics*, Vol. 1, MIT Press,
692 Cambridge, USA.
- 693 Noh, Y., Cheon, W.-G., Hong, S.-Y., and S. Raasch (2003), Improvement of the K-profile
694 model for the planetary boundary layer based on large eddy simulation data, *Boundary-*
695 *Layer Meteorol.*, *107*, 401–427.
- 696 Paulson, C. A., and J. D. Smith (1974), The AIDJEX lead experiment, *AIDJEX Bull.*,
697 *23*, 1–8.
- 698 Persson, P. O. G., Ruffieux, D., and C. W. Fairall (1997), Recalculations of pack ice and
699 lead surface energy budgets during the Arctic Leads Experiment (LEADEX) 1992, *J.*
700 *Geophys. Res.*, *102*, 25,085–25,089.
- 701 Pinto, J. O., Alam, A., Maslanik, J. A. Curry, J. A., and R. S. Stone (2003), Surface char-
702 acteristics and atmospheric footprint of springtime arctic leads at SHEBA, *J. Geophys.*
703 *Res.*, *108*, 8051, doi: 10.1029/2000JC000473.

- 704 Raasch, S., and G. Harbusch (2001), An Analysis of secondary circulations and their effects
705 caused by small-scale surface inhomogeneities using large-eddy simulation, *Boundary-*
706 *Layer Meteorol.*, *101*, 31–59.
- 707 Raasch, S., and M. Schröter (2001), A large-eddy simulation model performing on mas-
708 sively parallel computers, *Meteorol. Z.*, *10*, 363–372.
- 709 Ruffieux, D., Persson, P. O. G., Fairall, C. W., and D. E. Wolfe (1995), Ice pack and lead
710 surface energy budgets during LEADDEX 1992, *J. Geophys. Res.*, *100*, 4593–4612.
- 711 Schlünzen, K. H. (1988), Das mesoskalige Transport- und Strömungsmodell 'METRAS
712 - Grundlagen, Validierung, Anwendung, *Hamburger Geophysikalische Einzelschriften*,
713 *A88*, 139 pp.
- 714 Schlünzen, K. H. (1990), Numerical Studies on the inland penetration of sea breeze fronts
715 at a coastline with tidally flooded mudflats. *Beitr. Phys. Atmosph.*, *63*, 243–256.
- 716 Schröter, M., Bange, J., and S. Raasch (2000), Simulated airborne flux measurements in
717 a LES generated convective boundary layer, *Boundary-Layer Meteorol.*, *95*, 437–456.
- 718 Teixeira J., and S. Cheinet (2004) A simple mixing length formulation for the Eddy-
719 diffusivity parameterization of dry convection, *Boundary-Layer Meteorol.*, *110(3)*, 435–
720 453.
- 721 Troen, I. B., and L. Mahrt (1986), A simple model of the atmospheric boundary layer;
722 sensitivity to surface evaporation, *Boundary-Layer Meteorol.*, *37*, 129–148.
- 723 Turner, J. S. (1986), Turbulent entrainment: the development of the entrainment assump-
724 tion, and its application to geophysical flows, *J. Fluid Mech.*, *173*, 431–471.
- 725 Van Dop, H., and G. Verver (2001), Countergradient transport revisited, *J. Atmos. Sci.*,
726 *58*, 2240–2247.

- 727 Vihma, T., Hartmann, J., and C. Lüpkes (2003), A case study of an on-ice air flow over
728 the arctic marginal sea ice zone, *Boundary-layer Meteorol.*, *107*, 189–217.
- 729 Vihma, T., Lüpkes, C., J. Hartmann, and H. Sarvijärvi (2005), Observations and mod-
730 elling of cold-air advection over arctic sea ice in winter’, *Boundary-layer Meteorol.*,
731 *117(2)*, 275–300.
- 732 Wacker, U., Potty, K. V. J., Lüpkes, C., Hartmann, J., and M. Raschendorfer (2005),
733 A case study on a polar cold air outbreak over Fram Strait using a mesoscale weather
734 prediction model, *Boundary-layer meteorology*, *117(2)*, 301–336.
- 735 Weinbrecht, S., and S. Raasch (2001), High-resolution simulations of the turbulent flow
736 in the vicinity of an arctic lead, *J. Geophys. Res.*, *106 (C11)*, 27,035–27,046.
- 737 Zilitinkevich, S., V. Gryanik, V. Lykossov, and D. Mironov (1999), Third-order transport
738 and nonlocal turbulence closures for convective boundary layers. *J. Atmos. Sci.*, *56*,
739 3463–3477.
- 740 Zulauf, M.A., and S.K. Krueger (2003), Two-dimensional numerical simulations
741 of arctic leads: Plume penetration height, *J. Geophys. Res.*, *108(C2)*, 8050,
742 doi:10.1029/2003JC000495.

8. Tables and Figures

Table 1. Summary of modelled 'cold' cases (ABL temperature: 250 K). u and v are the lead-orthogonal and lead-parallel components of the geostrophic wind, F_s is the average surface heat flux over the lead, F_{100} and F_{200} are the maximum upward fluxes of sensible heat at 100 m and 200 m height, α_p is the plume inclination.

	case 1	case 2	case 3	case 4	case 5
	(weak-		(medium-	(strong-	
	(wind)		wind)	wind)	
u (m s ⁻¹)	3.0	4.0	5.0	7.0	10.0
v (m s ⁻¹)	-0.4	-1.0	-1.0	-2.0	-2.5
F_s (W m ⁻²)	123	155	170	223	270
F_{100} (W m ⁻²) (LES)	98	103	110	100	80
F_{100} (W m ⁻²) (METRAS)	88	92	95	98	90
F_{200} (W m ⁻²) (LES)	38	43	41	40	23
F_{200} (W m ⁻²) (METRAS)	42	42	41	42	40
α_p (degrees) (LES)	11.7	11.3	8.5	7.4	4.6
α_p (degrees) (METRAS)	11.3	11.0	8.0	6.3	4.6

Table 2. Summary of modelled 'warm' cases (ABL temperature: 260 K)

	case 1	case 2	case 3	case 4	case 5
	(weak-		(medium-	(strong-	
	(wind)		wind)	wind)	
u (ms ⁻¹)	3.0	4.0	5.0	7.0	10.0
v (ms ⁻¹)	-0.4	-1.0	-1.0	-2.0	-2.5
F_s (W m ⁻²)	51	61	72	89	121
F_{100} (W m ⁻²) (LES)	36	35	32	25	17
F_{100} (W m ⁻²) (METRAS)	28	31	31	30	30
F_{200} (W m ⁻²) (LES)	15	14	12	8	2
F_{200} (W m ⁻²) (METRAS)	12	12	13	12	11
α_p (degrees) (LES)	12.1	6.6	5.7	3.9	2.3
α_p (degrees) (METRAS)	10.6	6.6	4.9	3.6	3.0



Figure 1. Leads northeast of Svalbard (Aqua Modis image of 16 April 2005). The domain size is about 150 times 190 km².

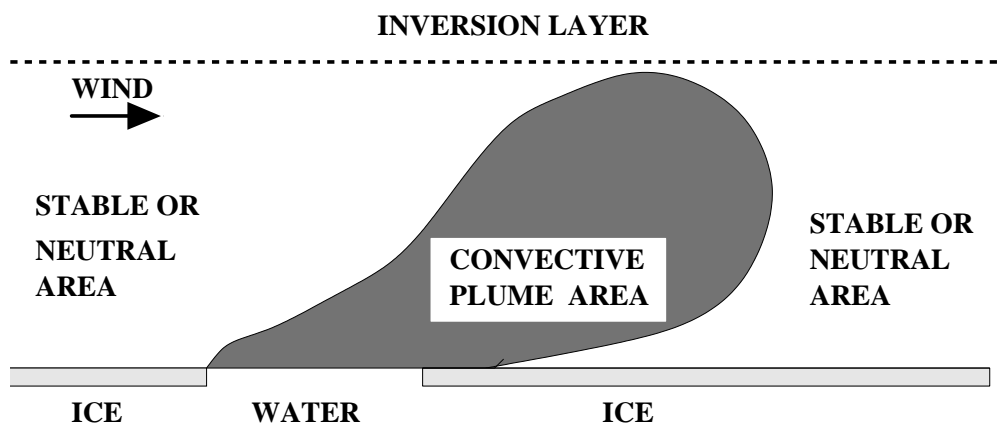


Figure 2. Schematic of the ABL over a polar lead during winter.

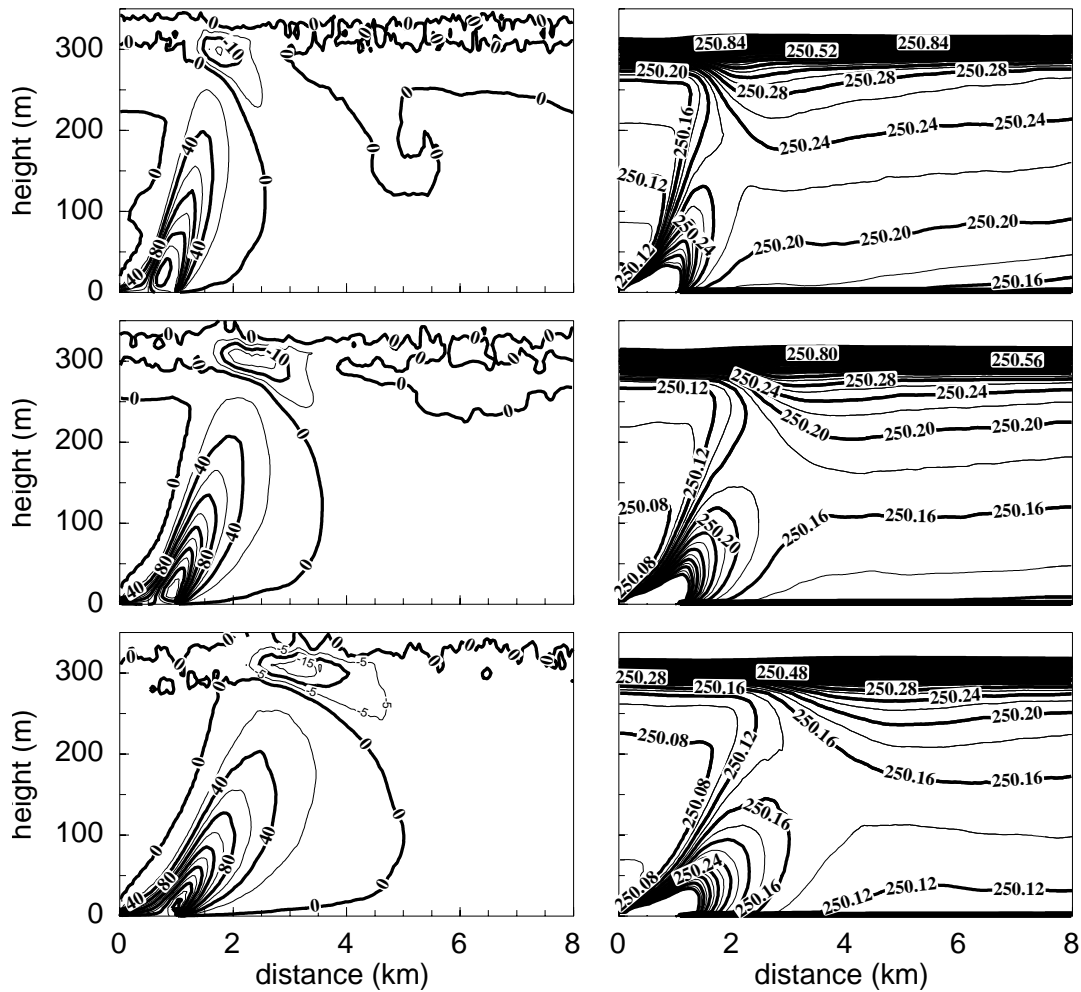


Figure 3. Sensible heat flux (left) in W m^{-2} and potential temperature in K (right) obtained from the LES model for the cold cases (top: weak-wind case, middle: medium-wind case, bottom: strong-wind case). The lead position is between 0 and 1 km distance. The surface wind is directed from left to right. The distance between contourlines is 5 W m^{-2} in case of downward fluxes.

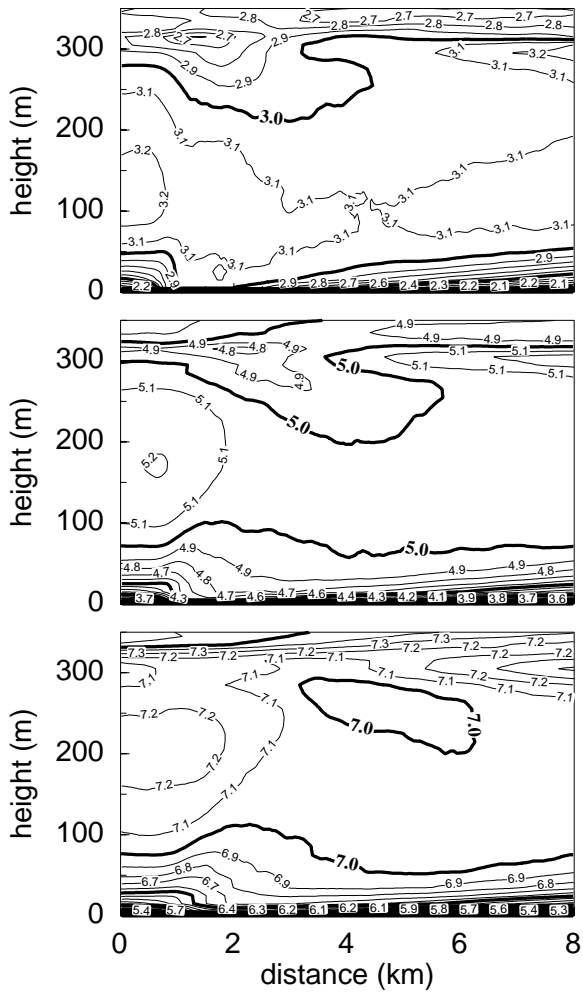


Figure 4. LES result as in Figure 3, but the absolute value of horizontal wind is shown in m s^{-1} .

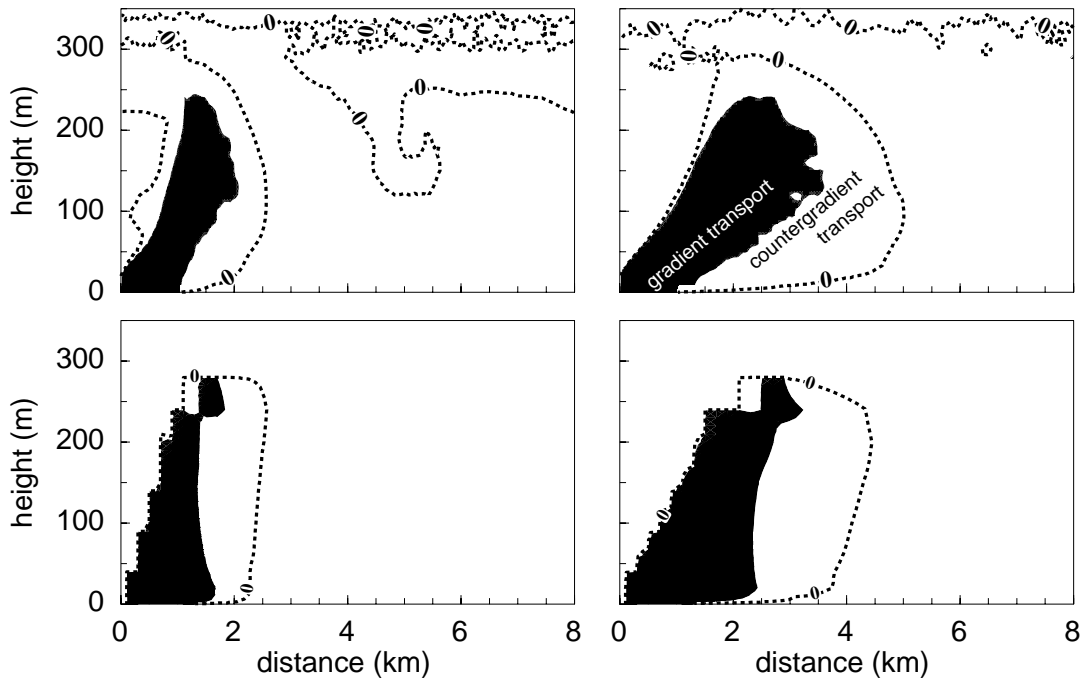


Figure 5. Regions with gradient and countergradient transport for the weak-wind (left) and strong-wind cold case (right) (top: LES, bottom: microscale model with the new closure of Section 5). The plume is defined as the area with upward heat flux (areas inside the dotted lines). In the dark areas the temperature decreases with height, everywhere else, it increases with height. Fluxes outside the plume are downward or zero.

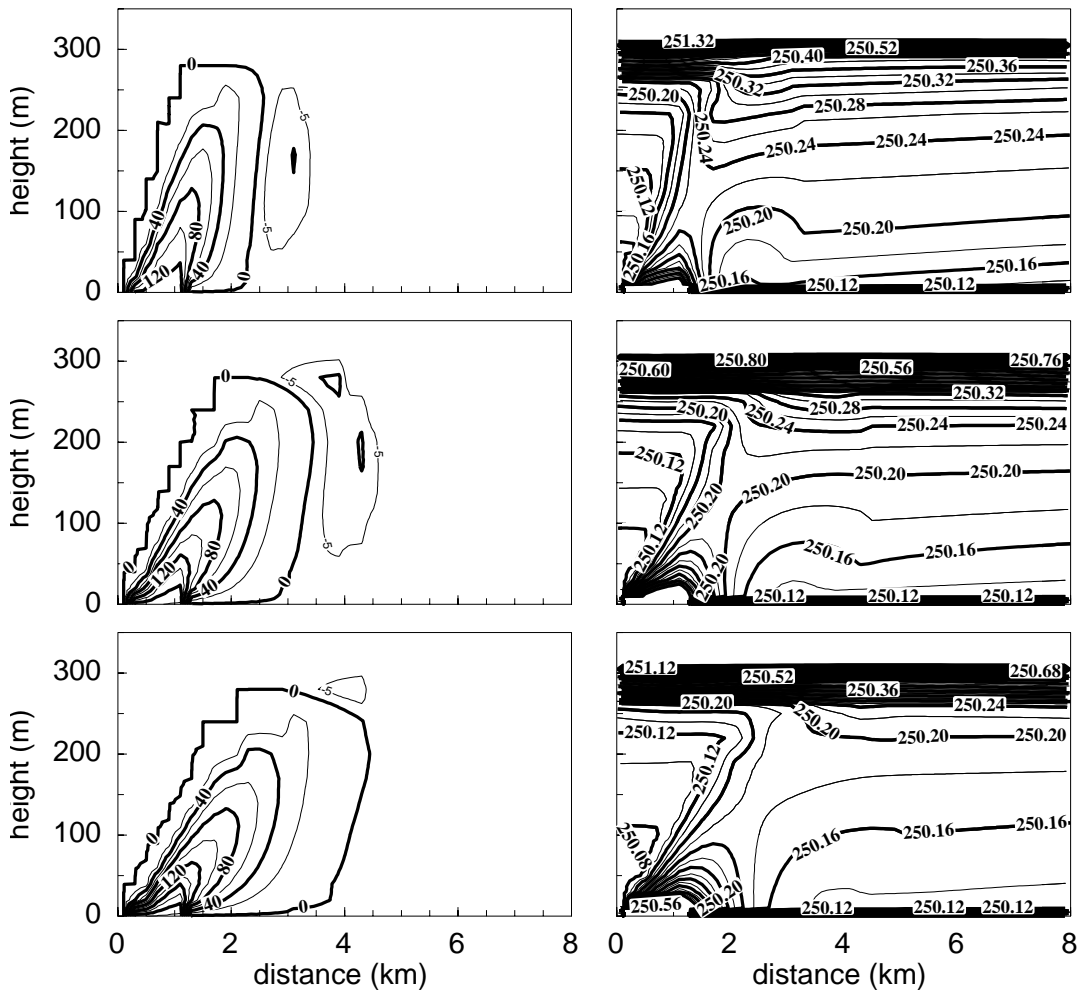


Figure 6. As Figure 3, but results were obtained with the microscale model using the new nonlocal closure derived in Section 5.

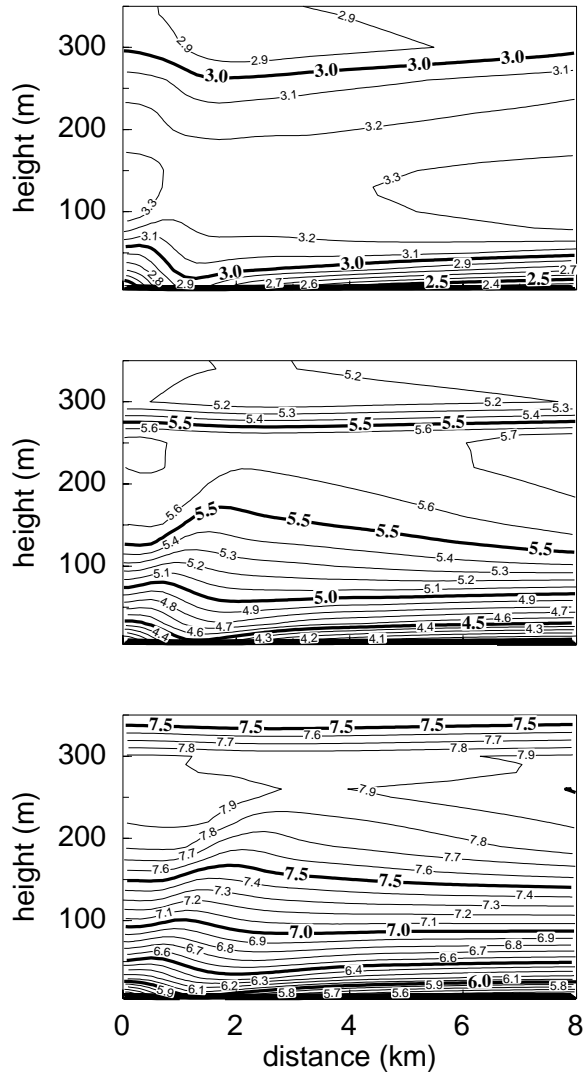


Figure 7. As Figure 6, but wind fields are shown (wind in m s^{-1}).

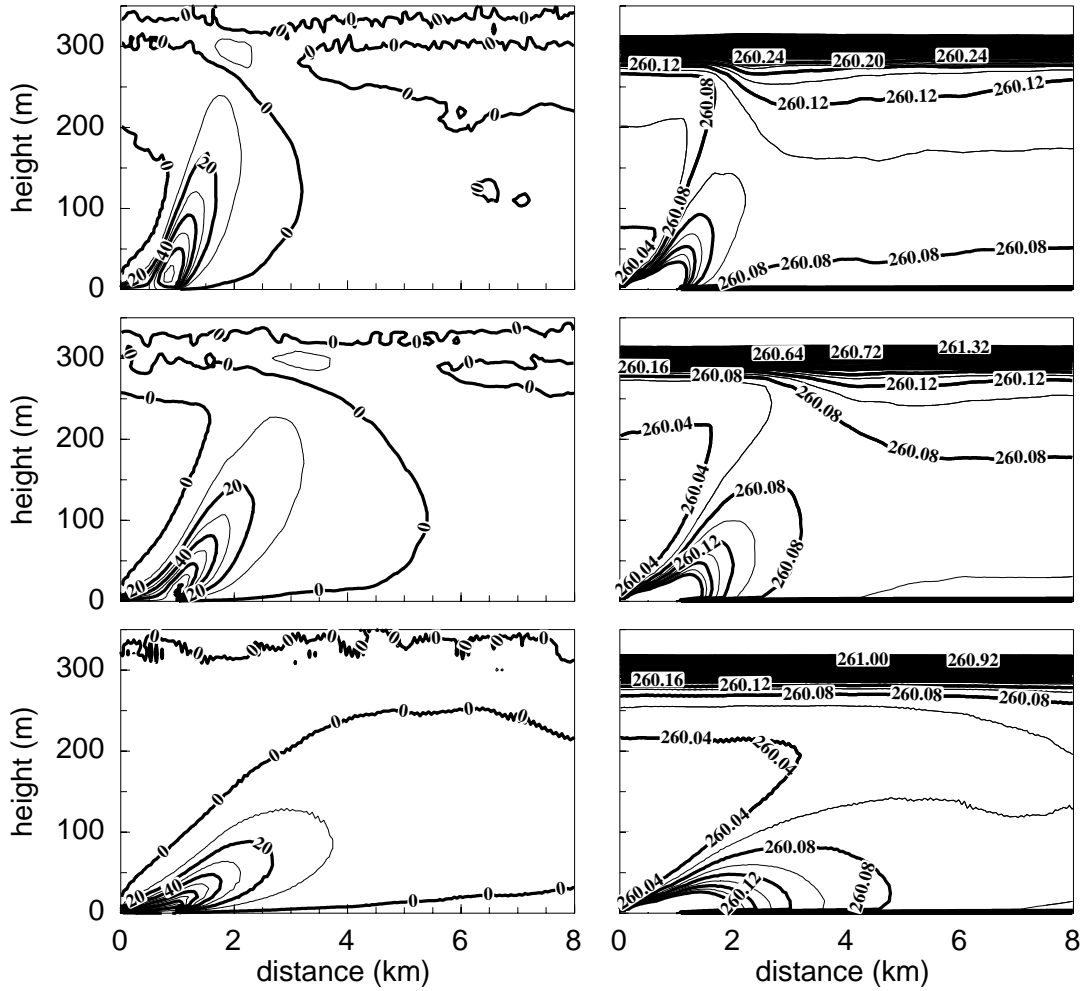


Figure 8. LES results as in Figure 3, but warm cases are shown.

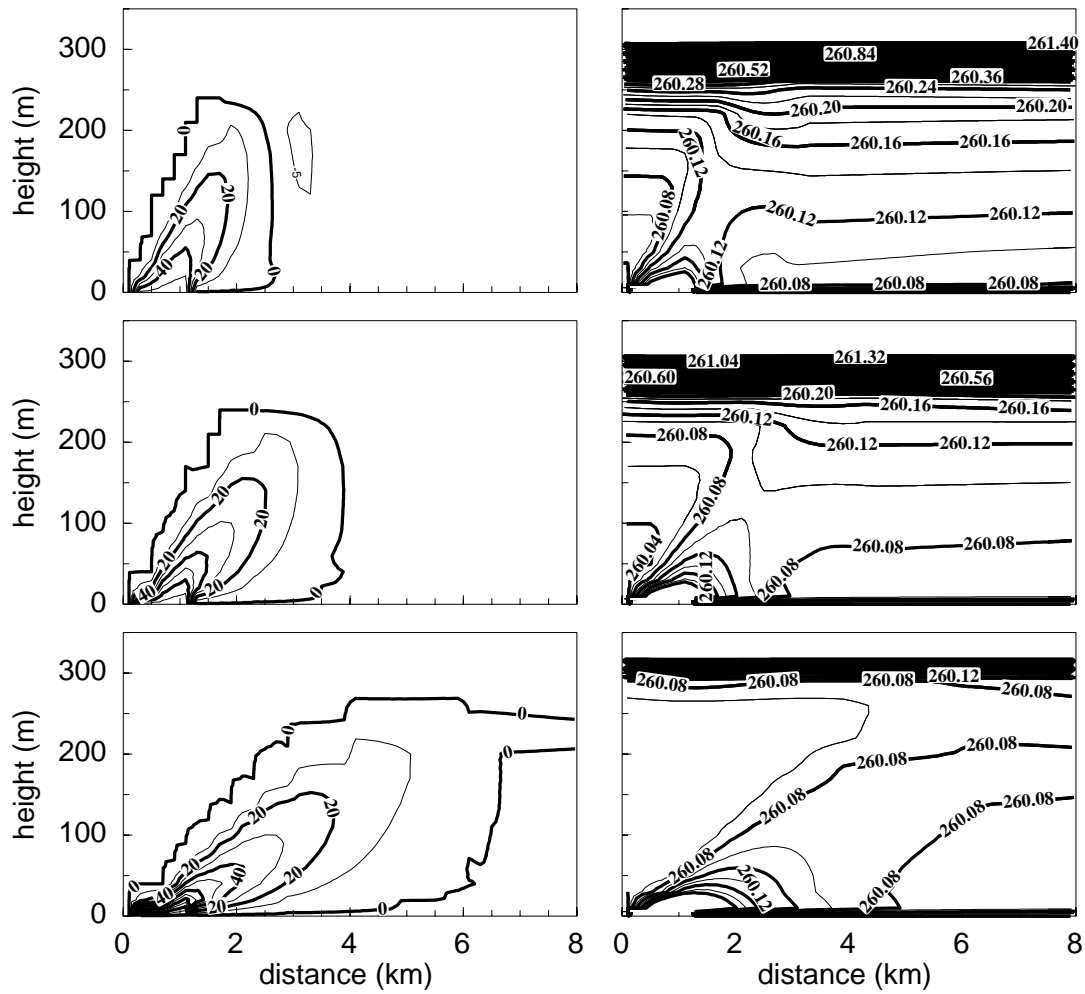


Figure 9. Results of the microscale model as in Figure 6, but warm cases are shown.

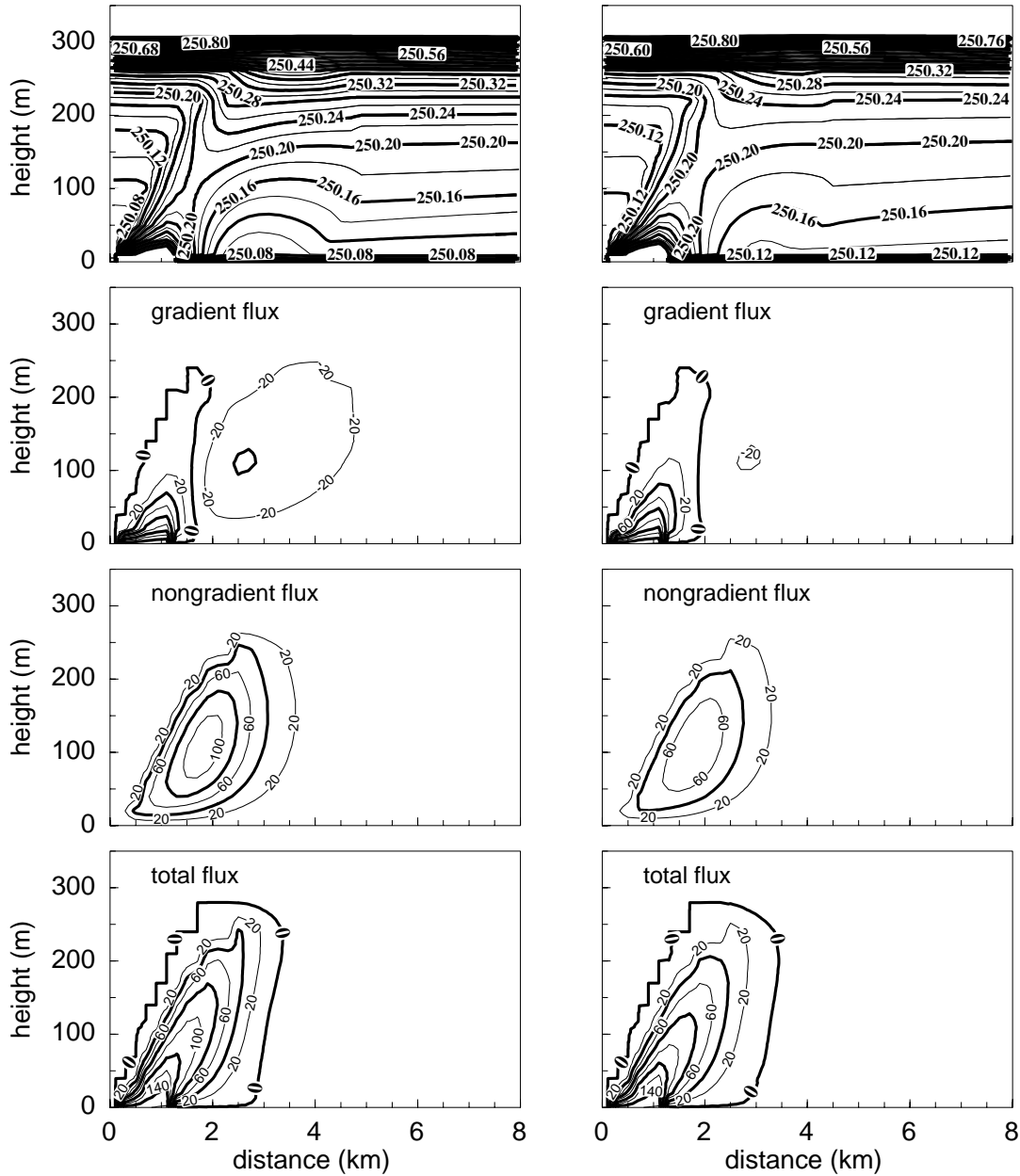


Figure 10. Results of the microscale model for the medium-wind cold case obtained with the new closure showing the sensitivity on the parameter b in the nonlocal term Γ given by equation (5) (left column: $b = 0.9$; right column: $b = 0.6$). Heat fluxes are given in W m^{-2} , pot. temperature in K .

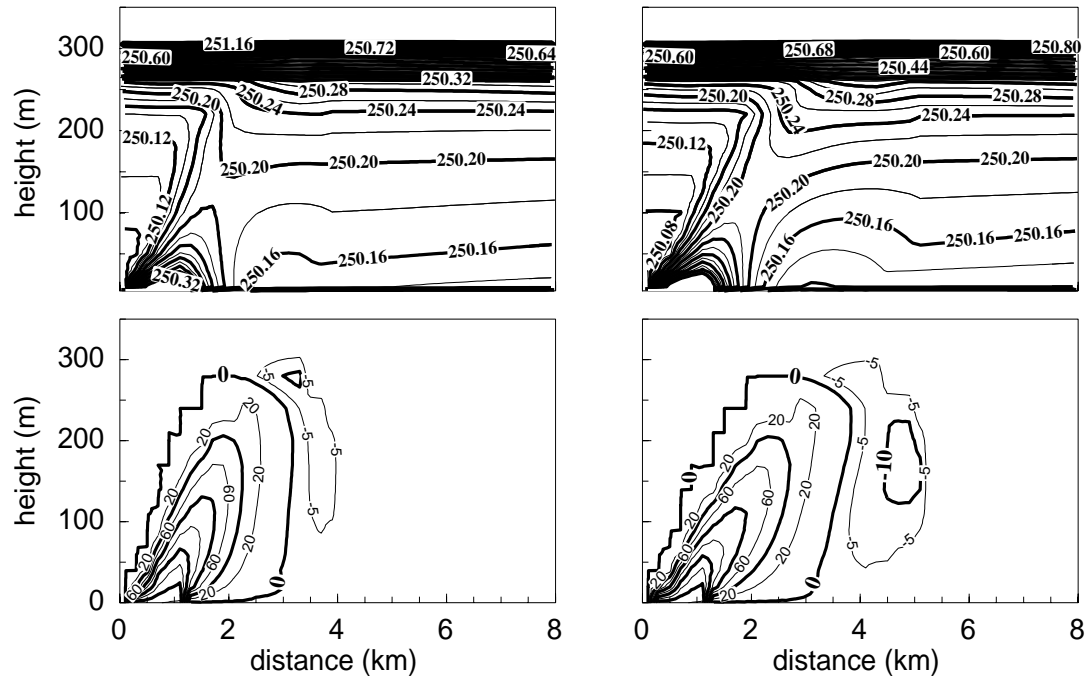


Figure 11. Results of the microscale model for the medium-wind cold case obtained with the new closure showing the sensitivity on the parameter a in equation (10) (left column: $a = 2.6$; right column: $a = 2.0$). Heat fluxes (bottom) are in W m^{-2} , pot. temperature (top) in K.

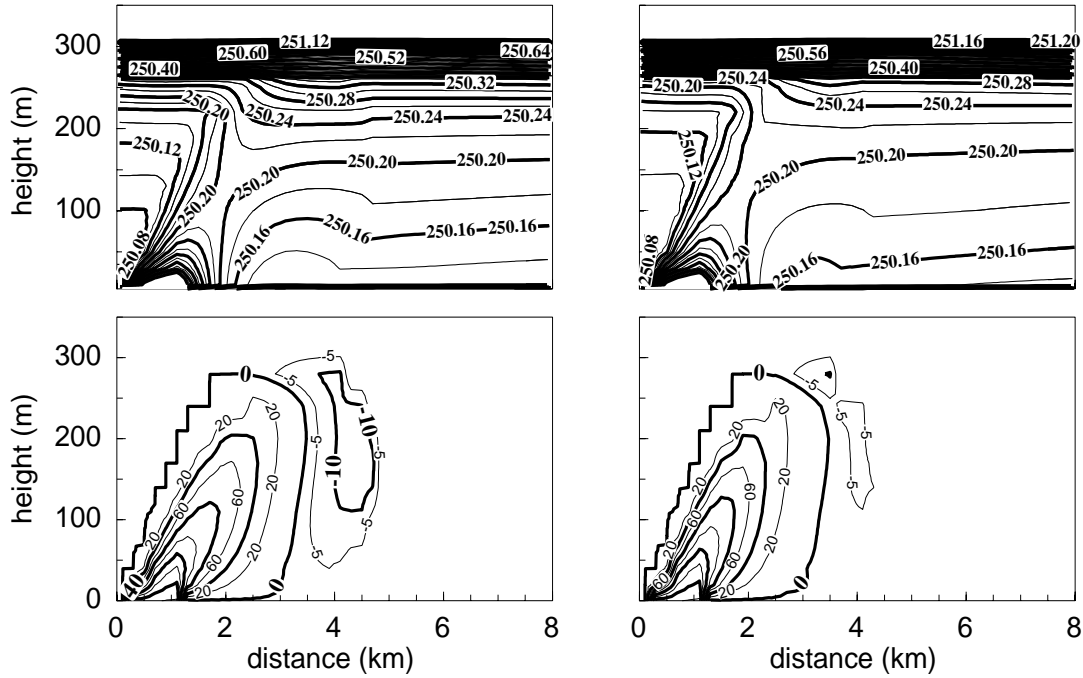


Figure 12. Results of the microscale model for the medium-wind cold case obtained with the new closure showing the sensitivity on the parameter c in equation (6) (left column: $c = 2.0$; right column: $c = 1.2$). Heat fluxes (bottom) are given in W m^{-2} , pot. temperature (top) in K.